PAPER

Check for updates

Mind the GAP: quantifying the breakdown of the linear vibronic coupling Hamiltonian†

Thomas J Penfold [ID] and Julien Eng [ID] *

Excited state dynamics play a critical role across a broad range of scientific fields. Importantly, the highly non-equilibrium nature of the states generated by photoexcitation means that excited state simulations should usually include an accurate description of the coupled electronic–nuclear motion, which often requires solving the time-dependent Schrödinger equation (TDSE). One of the biggest challenges for these simulations is the requirement to calculate the PES over which the nuclei evolve. An effective approach for addressing this challenge is to use the approximate linear vibronic coupling (LVC) Hamiltonian, which enables a model potential to be parameterised using relatively few quantum chemistry calculations. However, this approach is only valid provided there are no large amplitude motions in the excited state dynamics. In this paper we introduce and deploy a metric, the global anharmonicity parameter (GAP), which can be used to assess the accuracy of an LVC potential. Following its derivation, we illustrate its utility by applying it to three molecules exhibiting different rigidity in their excited states.

1 Introduction

Quantum dynamics simulations that seek to solve the time-dependent Schrödinger equation (TDSE) are crucial for describing processes occurring in electronically excited states and therefore are the key to understanding and refining the properties of functional molecules and materials across a range of applications, such as organic light emitting diodes (OLEDS)[1,2] and photovoltaics.[3–5] The equations of motion governing the dynamics occurring over excited state potential energy surfaces (PES) can be solved using either traditional grid based methods, such as the multi-configurational time-dependent Hartee (MCTDH) method[6,7] or trajectory based methods such as Tullys Trajectory Surface Hopping (TSH)[8,9] or Gaussian basis functions (GBFs) methods.[10–16] The latter being motivated by the original work of Heller,[17–19] which in contrast to TSH,[20,21] is able to retain a fully quantum description of the nuclear motion.

Independent of the method used to evolve the nuclear wavepacket, one of the major challenges in all of these simulations is obtaining an accurate description of the high-dimensional excited state PES upon which the nuclei evolve. One approach, primarily used for traditional grid based methods is to determine global analytic functions using quantum chemistry calculations.[22–24] These can be viewed as the non-Born Oppenheimer version of classical force fields and may be

refined using, for example, experimental data. This is the most accurate approach, but time consuming and extremely challenging for more than a few atoms due to the size of nuclear configuration space. For trajectory based methods, most approaches exploit the spatial locality of the trajectory making it possible to calculate PES *on-the-fly*, and so the complicated multidimensional potential can be calculated as and when it is required[25] removing the significant challenge of *a priori* computation of a PES. However, especially for larger molecules, this can still be challenging due to the computational scaling of the quantum chemistry methods and the large number of calculations required. The final approach, which is the focus of the present work, is to develop a model Hamiltonian, which are parameterised to match the PES around the important point on the PES, such as the Franck–Condon (FC) point. This reduces the number of quantum chemistry calculations required to map the excited state potential and can be a reliable way to calculate the excited state dynamics, especially when large amplitude motions in the excited state are absent.

In this work, we focus on the linear vibronic coupling (LVC) scheme developed by Köppel *et al.*[26,27] which describes the excited states of a system by a series of coupled shifted harmonic oscillators. Importantly, the simplicity of this approach makes it possible parameterise an effective Hamiltonian with very few quantum chemistry calculations,[28] providing a mechanism to achieve a detailed understanding of excited state dynamics through simplified models, which ultimately facilitates extraction of the critical parameters affecting function. These properties have recently been exploited to perform excited state dynamics using LVC models across a range of

Chemistry, School of Natural and Environmental Sciences, Newcastle University, Newcastle upon Tyne, NE1 7RU, UK. E-mail: julien.eng@newcastle.ac.uk

This journal is © the Owner Societies 2023

Phys. Chem. Chem. Phys., 2023, **25**, 7195–7204 | 7195

difference materials.[1,2,29–43] While the advantage of the LVC is that it can be relatively straightforward to obtain, the disadvantage is that it becomes inaccurate for larger displacements away from the starting geometry when anharmonic effects become more important. Consequently, in the present work introduce and deploy a metric, the Global Anharmonicity Parameter (GAP), which can used to assess the accuracy of an LVC potential. Following its derivation, we illustrate and discuss its utility by applying the method to three molecular systems.

2 Methodology

2.1 Computational details

Fig. 1 shows the molecules considered in the present work. Fig. 1a is a narrowband width blue fluorescent emitter used in OLEDS, named 2,5,8,11-tetra-*tert*-butylperylene (**TBPe**).[44] The rigidity of the molecule required to ensure the narrow emission spectrum makes it very suitable for the LVC treatment. Fig. 1b is a thermally activated delayed fluorescence[45,46] emitter exhibiting a D–A$_3$ structure with a triazatruxene central donor functionalized with three peripheral dibenzothiophene-*S,S*-dioxide acceptors abbreviated as **TAT-3DBTO$_2$** from now on.[47,48] Fig. 1c is **Maleimide** a small heterocyclic organic molecule previously studied using a quadratic vibronic coupling (QVC) Hamiltonian model.[49] The level of theory used for each molecule was chosen to correspond to previous works[48–50] and is described below.

All parameters required for the LVC Hamiltonian, described in Section 2.2, were extracted using the VCMaker software developed in-house and available for download at ref. 51. All quantum chemistry calculations described in the following subsections were all performed with the Q-Chem 5.0 software.[52,53]

2.1.1 TBPe. The minimum energy of the ground, first excited singlet (S$_1$) and triplet (T$_1$) states for **TBPe** (Fig. 1a) were optimised using density functional theory (DFT) and time-dependent density functional theory (TD-DFT) within the approximation of the PBE0 exchange and correlation functional.[54] Throughout the def2-TZVP basis set was used[55] and all TD-DFT simulations exploited the Tamm-Dancoff approximation.[56]

The Hessian of the electronic ground state and the Cartesian gradients of the first excited singlet (S$_1$) and triplet (T$_1$) states required for the LVC were computed at the ground state

optimised geometry using the same level of theory described above. All calculations were performed in the gas phase. Cartesian coordinates of the ground and excited states optimised geometries are provided in Tables S1, S2 and S4 (ESI†).

2.1.2 TAT-3DBTO$_2$. The electronic structure of **TAT-3DBTO$_2$** (Fig. 1b) has been previously studied by Eng *et al.*[48] Here the ground and excited state geometry optimisations were performed with the DFT and TD-DFT approaches within the approximation of the range-separated LRC-ωPBEh functional.[57] A 6-31G* basis set[58–60] was used throughout and all of the TD-DFT simulations were performed within the Tamm–Dancoff approximation.[56] Throughout the range-separation parameter ω was fitted using the optimal tuning approach described in ref. 61–64. The geometry optimisation, Hessian and gradient calculations were all performed in the gas phase. Cartesian coordinates of the ground and excited states optimised geometries of **TAT-3DBTO$_2$** are reported in Tables S10, S12 and S14 (ESI†).

2.1.3 Maleimide. Geometry optimisations and excited state calculations of **Maleimide** (1c) have followed the recent work of Lehr *et al.*[49] and have been performed using the Equation of Motion Coupled Cluster Singles and Doubles (EOM-CCSD) approach and a cc-pVDZ basis set.[65] Cartesian coordinates of the ground and excited states optimised geometries of **Maleimide** are reported in Tables S17 and S18 (ESI†).

2.2 Linear vibronic coupling

The electronic diabatic Hamiltonian elements $W_{n,n}$ can be expressed by expanding $\mathbf{W} - V_0\mathbf{1}$ as a Taylor series expansion of the diabatic potential around a reference nuclear geometry (Q_0), usually the FC geometry. V_0 is a reference potential chosen accordingly to the problem. It is not restricted to a particular form but is often defined as harmonic with vibrational frequencies ω_i along dimensionless normal coordinates Q_i. In this case, Hamiltonian elements are expressed:

$$W_{n,m} - V_0\delta_{nm} = \varepsilon_n\delta_{nm} + \sum_i^{3N-6} \left.\frac{\partial W_{n,m}}{\partial Q_i}\right|_{Q_0} Q_i + \frac{1}{2!}\sum_{i,j}^{3N-6} \left.\frac{\partial^2 W_{n,m}}{\partial Q_i \partial Q_j}\right|_{Q_0} Q_i Q_j \quad (1)$$

where δ_{nm} is the Kronecker delta. Q_i denotes the $3N - 6$ dimensionless normal coordinates related to the normal modes of vibration, N being the number of atoms. V_0, within the harmonic approximation is expressed:

$$V_0 = \frac{1}{2}\omega_i Q_i^2 \quad (2)$$

and the kinetic energy operator therefore takes the form:

$$\hat{T}_N = -\sum_i \frac{1}{2}\omega_i \frac{\partial^2}{\partial Q_i^2} \quad (3)$$

Within the LVC scheme, the Taylor expansion of the diabatic potential energy to the first order, the so-called LVC model
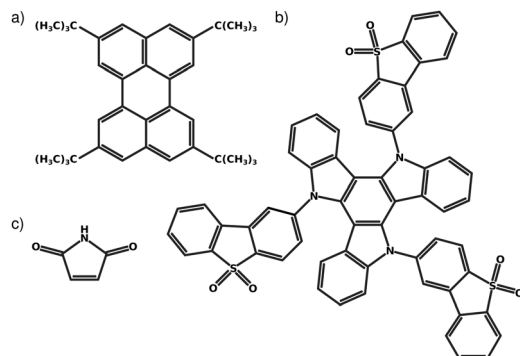

Fig. 1 Structure of (a) **TAT-3DBTO$_2$** (b) **TBPe** and (c) **Maleimide**.

7196 | *Phys. Chem. Chem. Phys.*, 2023, **25**, 7195–7204

This journal is © the Owner Societies 2023

Hamiltonian, is written:

$$W_{n,m} - V_0 \delta_{nm} = \varepsilon_n \delta_{nm} + \sum_i^{3N-6} \frac{\partial W_{n,m}}{\partial Q_i}\bigg|_{Q_0} Q_i \qquad (4)$$

The diabatic electronic states are built such as they coincide to the adiabatic electronic states at FC (Q_0). We introduce the notation:

$$\kappa_i^{(n)} = \frac{\partial W_{n,n}}{\partial Q_i}\bigg|_{Q_0} \qquad (5)$$

and

$$\lambda_j^{(n,m)} = \frac{\partial W_{n,m}}{\partial Q_j}\bigg|_{Q_0} \qquad (6)$$

where κ_i and $\lambda_j^{n,m}$ are the intra- and inter-state coupling, respectively. The on-diagonal elements (κ_i) are the forces acting within an electronic surface and are responsible for structural changes of excited-state potentials compared to the ground state. They are therefore responsible for the reorganization energy and often referred to as the tuning modes. The off-diagonal elements ($\lambda_j^{n,m}$) are the couplings responsible for transferring wavepacket population between different excited states and consequently are usually referred to as coupling modes. For $m = n$, eqn (4) can then be reorganised such as:

$$W_{n,n} = \varepsilon_n + \sum_i \left[\frac{1}{2}\omega_i \left(Q_i + \frac{\kappa_i^{(n)}}{\omega_i} \right)^2 - \frac{\kappa_i^{(n)2}}{2\omega_i} \right] \qquad (7)$$

This equation emphasizes the roles of the intrastate coupling constant $\kappa_i^{(n)}$ in shifting the diabatic potential in energy $\left(\delta E_i = -\frac{\kappa_i^{(n)2}}{2\omega_i} \right)$ and in position $\left(\delta Q_i^{(n)} = -\frac{\kappa_i^{(n)}}{\omega_i} \right)$.

Within the LVC, the minimum of any excited state PES n is given by

$$Q_{\text{LVC}}^{(n)} = Q_0 + \sum_i^{3N-6} \delta Q_i^{(n)} \qquad (8)$$

and in the limit that the harmonic approximation is valid, corresponds to the exact minimum of the PES $Q_{\text{Min}}^{(n)}$. If there is significant anharmonicity, $Q_{\text{LVC}}^{(n)}$ and $Q_{\text{Min}}^{(n)}$ becomes significantly different.

Eqn (8) can be rewritten in term of κ:

$$Q_{\text{LVC}}^{(n)} = Q_0 + \sum_i^{3N-6} \frac{-\kappa_i^{(n)}}{\omega_i} \qquad (9)$$

This demonstrates that an alternative method for estimating $\kappa^{(n)}$ can be obtained as the difference between the excited state harmonic minimum geometry and the FC geometry:

$$\sum_i^{3N-6} \frac{\kappa_i^{(n)}}{\omega_i} = Q_0 - Q_{\text{LVC}}^{(n)}. \qquad (10)$$

If $Q_{\text{LVC}}^{(n)}$ is replaced by $Q_{\text{Min}}^{(n)}$, i.e. the exact minimum of excited state n, one obtains a second set of κ parameters: $\kappa_i^{*(n)}$:

$$\sum_i^{3N-6} \frac{\kappa_i^{*(n)}}{\omega_i} = Q_0 - Q_{\text{Min}}^{(n)}. \qquad (11)$$

While the estimation method of $\kappa_i^{(n)}$ based on the gradient at FC probes vertically the topology of the PES, estimating $\kappa_i^{*(n)}$ based on the excited state minima provides information at potentially larger displacements from FC. Crucially, comparing $\kappa_i^{(n)}$ and $\kappa_i^{*(n)}$ provides a direct estimate of the validity of the LVC model, i.e. in the limit the harmonic approximation holds, $\kappa_i^{(n)} = \kappa_i^{*(n)}$.

In this work we seek to develop a simple general parameter which can be used to characterise how suitable the LVC approach is. The global anharmonicity parameter (GAP) is defined as:

$$\Xi^{(n)} = \frac{K_+^{(n)} - K_-^{(n)}}{K_+^{(n)}} \times 100 \qquad (12)$$

where

$$K_+^{(n)} = \text{Max}\left(\sum_i^{3N-6} \left|\kappa_i^{(n)}\right|, \sum_i^{3N-6} \left|\kappa_i^{*,(n)}\right| \right) \qquad (13)$$

and

$$K_-^{(n)} = \text{Min}\left(\sum_i^{3N-6} \left|\kappa_i^{(n)}\right|, \sum_i^{3N-6} \left|\kappa_i^{*,(n)}\right| \right). \qquad (14)$$

Ξ takes values from 0% to 100% where Ξ = 0% corresponds to a scenario where the molecule is rigid and the theoretical LVC minimum corresponds to the real minimum and Ξ = 100% where the molecule is flexible and the harmonic oscillator approximation is no longer valid.

As these parameters are all calculated in terms of individual normal mode, Ξ can be represented in term of relative single mode anharmonicity (RSMA) ξ_i^n:

$$\xi_i^{(n)} = \frac{1}{\alpha^{(n)}} \left(\kappa_i^{(n)} - \kappa_i^{*,(n)} \right) \qquad (15)$$

where α is a normalisation coefficient:

$$\alpha^n = \sum_i^{3N-6} \left(\kappa_i^{(n)} - \kappa_i^{*,(n)} \right) \qquad (16)$$

The GAP and its individual normal mode breakdown will be used throughout this work.

3 Results

3.1 TBPe

As described above, **TBPe** (Fig. 1a) is a narrowband fluorescent emitter[44] and given the rigidity required in the molecular structure to achieve narrow emission spectra[66] one would expect the LVC model to provide an accurate description of TBPe excited states. In this section we focus on the lowest excited triplet (T_1) and singlet (S_1) states which both exhibit $\pi \to \pi^*$ excitation localised on the central aromatic moiety of **TBPe**. Fig. S1 (ESI†) shows the difference of electronic density associated to the $S_1 \leftarrow GS$ and $T_1 \leftarrow GS$ transitions. The minimum energy geometry of both of these states exhibit very small root-mean square deviation (RMSD: Θ) with respect to

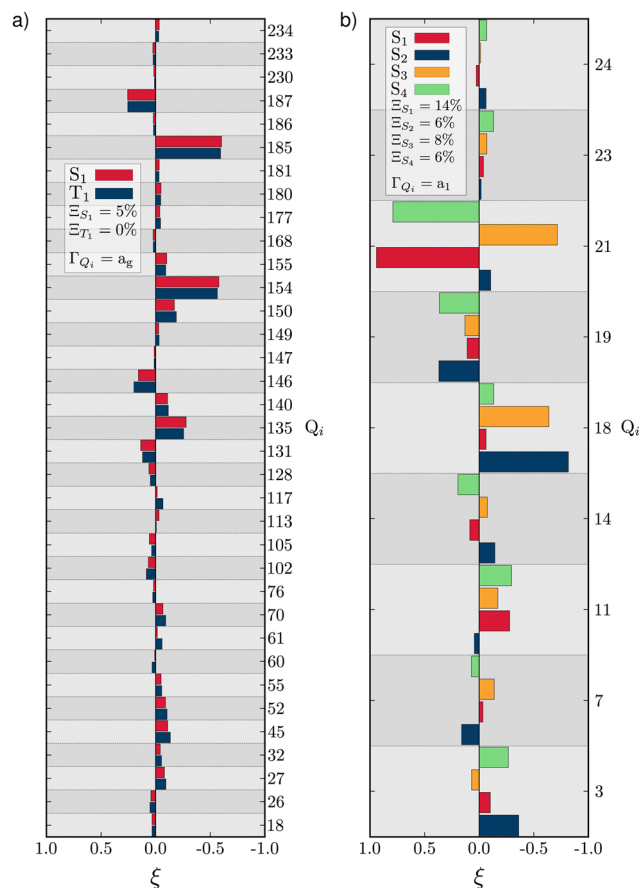This journal is © the Owner Societies 2023

Phys. Chem. Chem. Phys., 2023, **25**, 7195–7204 | 7197

Fig. 2 RSMA (ξ) for **TBPe** S_1 and T_1 (a) and **Maleimide** S_1, S_2, S_3 and S_4 (b). GAPs are shown inset. Only fully symmetric normal modes are shown. ξ for normal modes of other symmetries are shown in Tables S6 and S7 (ESI†) for **TBPe** and Tables S21, S22, S24 and S25 (ESI†) for **Maleimide**.

the electronic ground state optimised geometry of $\Theta(S_1^{Min}, GS) = 0.025$ Å and $\Theta(T_1^{Min}, GS) = 0.029$ Å, respectively.

Fig. 2a shows the GAP (Ξ) and RSMA (ξ) for the S_1 and T_1 excited states of TBPe. The GAP of $\Xi^{S_1} = 5.2\%$ and $\Xi^{T_1} = 0.4\%$ confirms, consistent with the rigidity discussed above, the validity of the Harmonic approximation for this molecule. The RSMA shown in Fig. 2a highlights the discrete normal modes with the largest RSMA, which are in-plane motions (high frequency). Out-of-plane distortions have smaller RSMA because such motions involve a bending of the π-system which requires more energy than a collective in-plane vibration of the C–C bonds. The largest RSMA for the S_1 and T_1 states coincide, reflecting the similar character of the excited states.

The validity of the GAP (Ξ) approach is confirmed by the small RMSD between the optimised structures of the S_1 and T_1 states discussed above. In addition, the theoretical minima obtained using the displacement harmonic oscillator approach: *i.e.* S_1^{LVC} and T_1^{LVC}, respectively are in very close agreement with the true minima with the RMSD of the triplet state being $\Theta(T_1^{Min}, T_1^{LVC}) = 0.006$ Å and $\Theta(S_1^{Min}, S_1^{LVC}) = 0.016$ Å for the singlet state. A small nuclear distortion alone is not sufficient to confirm the validity of the harmonic approximation. The

relaxation energy obtained from κ: $\Delta E^{(n)} = \sum_i \frac{\kappa_i^{(n)2}}{\omega_i}$ and from

κ^*: $\Delta E^{*,(n)} = \sum_i \frac{\kappa_i^{*,(n)2}}{\omega_i}$ for S_1 and T_1 are quantitatively the same: $\Delta E^{(S_1)} = -0.157$ eV, $\Delta E^{*,(S_1)} = -0.135$ eV and $\Delta E^{(T_1)} = -0.272$ eV, $\Delta E^{*,(T_1)} = -0.269$ eV and in good agreement to the relaxation energy between the ground state optimised geometry and S_1^{Min} $\left(\Delta E^{S_1^{Min}} = -0.167 \text{ eV}\right)$ and T_1^{Min} $\left(\Delta E^{T_1^{Min}} = -0.270 \text{ eV}\right)$.

The quality of the structure and energy of the state of interest is important, however the overall electronic structure at the LVC minimum is also required to be in good agreement to the optimised minimum. Table 1 shows the comparison between the electronic structure of TBPe at the two optimised geometries S_1^{Min} and T_1^{Min} and their respective LVC geometries: S_1^{LVC} and T_1^{LVC}. At both S_1^{Min} and T_1^{Min} the energy of S_1 is very well reproduced by the LVC generated geometry with a difference of energy < 0.005 eV. The energy of T_1 also shows good agreement between the optimised and the LVC minima with only a small difference in energy of 0.01 eV between S_1^{Min} and S_1^{LVC}. The maximal difference of energy is observed for the ground state energy S_1^{Min} and S_1^{LVC} with a difference of 0.02 eV. This is due mainly to the difference in the shape of the PES where S_1 and T_1 might feature shallower PES than the ground state. While this difference is negligible, it shows that for less rigid system the energetics of neighbouring states might not be is such a good agreement to the optimised minimum.

3.2 TAT-3DBTO$_2$

Triazatruxene tris(dibenzothiophene-*S,S*-dioxide) **TAT-3DBTO$_2$** is a promising candidate for application in TADF OLEDs.[47] It consists of a central donor moiety linked to three peripherals acceptor units through carbon–nitrogen single bonds (see Fig. 1). This type of donor–acceptor molecule features low-lying charge transfer (CT) states that typically exhibit small singlet–triplet energy gap, a requirement for the up-conversion of non-emissive triplet states in TADF.[45] Indeed, after excitation

Table 1 The excited state energies and oscillator strengths of **TBPe** at the true and LVC minimum energy geometries of the S_1 and T_1 states

State	S_1^{Min}		S_1^{LVC}	
	f	ΔE/eV	f	ΔE/eV
S_0	—	0.13	—	0.15
T_1	—	1.65	—	1.64
S_1	0.587	2.98	0.594	2.98
T_2	—	3.08	—	3.09
T_3	—	3.31	—	3.32

State	T_1^{Min}		T_1^{LVC}	
	f	ΔE/eV	f	ΔE/eV
S_0	—	0.26	—	0.27
T_1	—	1.62	—	1.62
S_1	0.594	3.01	0.617	3.01
T_2	—	3.13	—	3.13
T_3	—	3.38	—	3.39

7198 | *Phys. Chem. Chem. Phys.*, 2023, **25**, 7195–7204

This journal is © the Owner Societies 2023

the acceptor units can rotate with respect to the central donor moiety around the C–N bond (φ_i, see Fig. S2, ESI†) to accommodate the excited state electronic density and minimise the orbital overlap. This relaxation effectively reduces the energy gap between singlet and triplet CT states that is desirable for efficient TADF emitters.

Large amplitude motions, and in particular rotations, are typically situations where harmonic potentials breakdown. At the geometry of the ground state minimum, **TAT-3DBTO$_2$** features a C_3 symmetry where all three acceptors are tilted by $\varphi = 57.29$ deg with respect to the central moiety. At this geometry, the lowest triplet state T$_1$ at $E(\text{T}_1) = 3.09$ eV is a mix of local excitation focused on the donor and charge transfer (CT) towards all the acceptors units. In contrast, the S$_1$ state ($E(\text{S}_1) = 3.62$ eV) is a pure CT from the donor to all acceptors. The electronic structure of **TAT-3DBTO$_2$** at the ground state optimised geometry is reported in Table 2 and the difference of electronic density of S$_1$ and T$_1$ are shown in Fig. S3 (ESI†). Relaxation after excitation into S$_1$ leads to a localisation[67] of the CT towards a single acceptor and a stabilisation of the state to $E(\text{S}_1) = 3.32$ eV (see Table 2 top right). The acceptor involved in the CT of S$_1$ rotates around the donor–acceptor bond to a more perpendicular orientation with $\varphi_1 = 77.47$ deg. The other two acceptors are not involved in the excitation, remaining tilted with $\varphi_2 = 61.04$ deg and $\varphi_3 = 59.84$ deg. The nature of T$_1$ changes during the relaxation in S$_1$ to become a mixed charge

transfer/locally excited state based upon the acceptor, ^{3}CT/^{3}LE(A) state at $E(\text{T}_1) = 3.14$ eV. We report the reader to the work of Eng et al.[48] for a more detailed analysis of the electronic structure.

The GAP for S$_1$ is $\varXi_{\text{S}_1} = 86\%$ and therefore clearly reflects a significant breakdown of the LVC model. Due to symmetry, only fully symmetric normal modes can have $\kappa \neq 0$, i.e. a non-zero gradient at the FC geometry and therefore the κ values calculated using the LVC will not be able to capture the symmetry breaking. In addition, because the κ^* values are estimated at a structure with no symmetry (S$_1^{\text{Min}}$) it does not have the same constraint and may exhibit non-zero gradient along any normal modes. This is demonstrated in Fig. S4 (ESI†) as normal modes that are not a$_1$ show non negligible RSMA. Consequently, we could expect the LVC minimum to be similar to the optimised geometry of S$_1$ within the C_3 point group symmetry (S$_1^{\text{Sym}}$), discussed in ref. 67. The electronic structure at S$_1^{\text{Sym}}$ is shown in Table 2 bottom left. The electronic structure at this geometry is similar as the electronic structure at GS but with the lowest excited states closer in energy. The interest of this critical structure for TADF is discussed in more details in the work of Eng et al.[67] The degeneracy of states due to the C_3 point group symmetry is maintained and S$_1$ is stabilised to $E(\text{S}_1) = 3.50$ eV and T$_1$ is found at $E(\text{T}_1) = 3.19$ eV. The GAP of S$_1$ considering the set κ^* taken from the S$_1^{\text{Sym}}$ geometry $\varXi_{\text{S}_1}^{\text{Sym}} = 69\%$ is slightly lower than $\varXi_{\text{S}_1}$ but not sufficiently to validate the harmonic approximation.

This analysis demonstrates that symmetry breaking is not the only reason for the breakdown of the harmonic approximation in **TAT-3DBTO$_2$**. The rotational motion involved in the relaxation is not well described by normal modes of vibrations and the normal modes at the S$_1$ minimum are too different from the set of normal modes at the FC geometry. The LVC minimum of S$_1$ (S$_1^{\text{LVC}}$) shows torsion angles ($\varphi_1 = 66.59$ deg, $\varphi_2 = 62.88$ deg and $\varphi_3 = 60.98$ deg) closer to the ones of the structure of S$_1^{\text{Min}}$. While S$_1^{\text{LVC}}$ shows an electronic structure that retains, considering numerical errors, the degeneracy pattern of the C_3 symmetry with the good ordering of the electronic states, see Table 2 bottom right, the energies of the electronic states, and especially the energy of S$_1$, are however aberrant and reflect the non-physical nature of the structure.

Compared to the S$_1$ state, the GAP of the T$_1$ state is smaller: $\varXi_{\text{T}_1} = 53\%$. This is due to the predominantly LE nature of T$_1$ at the ground state optimised geometry. $\pi \rightarrow \pi$ excitation typically lead to bond length reorganisation that involves small nuclear distortions resulting in small GAP as observed in TBPe. The mixed nature of the state means the excitation is delocalised over both the acceptors and the donor units. Modulation of the orbital overlap to minimise the state energy occurs via donor–acceptor rotation. This effect alone is not sufficient to explain the large $\varXi_{\text{T}_1}$, in particular as torsion angle is similar for the ground state optimised geometry and the minimum of T$_1$, i.e. $\varphi_{1,2,3} = 57.29$ deg and $\varphi_1 = 52.51$ deg, $\varphi_2 = 54.47$ deg, $\varphi_3 = 50.88$ deg, respectively. The value of the torsion coordinates φ is reported for all geometries in Table S9 (ESI†). We attribute the large anharmonicity to the change of nature of the state from a

Table 2 Electronic structure of **TAT-3DBTO$_2$** at the ground state optimised geometry (top left), the geometry of S$_1$ minimum (top right), the C_3 symmetry minimum of S$_1$ (bottom left) and the S$_1$ LVC minimum (bottom right). All energies are given in eV and relative to the energy of the electronic ground state at the ground states optimised geometry. f stands for oscillator strength

GS			S$_1^{\text{Min}}$		
State	f	ΔE/eV	State	f	ΔE/eV
S$_0$	—	0.00	S$_0$	—	0.42
T$_1$	—	3.09	T$_1$	—	3.14
T$_2$/T$_3$	—	3.19	S$_1$	0.004	3.32
T$_4$	—	3.23	T$_2$	—	3.36
T$_5$/T$_6$	—	3.42	T$_3$	—	3.45
T$_7$	—	3.51	T$_4$	—	3.61
S$_1$	0.005	3.62	T$_5$	—	3.62
T$_8$/T$_9$	—	3.67	T$_6$	—	3.65
T$_{10}$	—	3.67	S$_2$	0.013	3.68
S$_2$/S$_3$	0.184	3.67	T$_7$	—	3.78

S$_1^{\text{Sym}}$			S$_1^{\text{LVC}}$		
State	f	ΔE/eV	State	f	ΔE/eV
S$_0$	—	0.18	S$_0$	—	0.46
T$_1$	—	3.19	T$_1$	—	3.39
T$_2$/T$_3$	—	3.23	T$_2$	—	3.44
T$_4$	—	3.30	T$_3$	—	3.47
T$_5$/T$_6$	—	3.48	T$_4$	—	3.54
S$_1$	0.000	3.50	T$_5$	—	3.71
S$_2$/S$_3$	0.046	3.52	T$_6$	—	3.73
T$_7$	—	3.53	S$_1$	0.036	3.74
T$_8$/T$_9$	—	3.60	T$_7$	—	3.78
			S$_2$	0.048	3.80
			S$_3$	0.092	3.83

This journal is © the Owner Societies 2023

Phys. Chem. Chem. Phys., 2023, **25**, 7195–7204 | **7199**

LE/CT mixed nature at FC geometry to a LE(A) at the T_1 minimum. The κ parameters extracted from the electronic gradient at FC describe the mixed nature of T_1, while the $\kappa^\star$ extracted from the difference of geometry, describe the diabatic ^{3}LE(A) excited state.

The analysis of the RSMA (Fig. S4, ESI†) confirms the difference nature of S_1 and T_1. Indeed the normal modes with the largest ξ in S_1 are normal modes within the 1000 cm^{-1} to 1200 cm^{-1} (from mode Q_{163} to Q_{201}) range that are typically out of plane motions such as rotations and bending. Such motions are representative of the large localisation of the excitation occurring in S_1. Conversely, the largest ξ in the T_1 state are found to be normal modes with frequencies between 1600 cm^{-1} and 1700 cm^{-1} (from mode Q_{165} to Q_{194}) and are C–C and C=C bond stretching vibrations that are involved in the π system reorganisation that occurs during the relaxation in a $\pi \rightarrow \pi^\star$ electronic state.

3.3 Maleimide

Small heterocyclic organic compounds are ideal test systems for probing theoretical concepts in photochemistry and photophysics. In this context maleimides have gained increasing interest over the past years due to a wide variety of potential applications.[68–71] Recently Worth *et al.*[49] have studied the excited state dynamics of **Maleimide** (see Fig. 1c) using a QVC Hamiltonian. By including four low-lying singlet excited states within the manifold of 24 vibrational modes they were able to provide a detail insight into the excited state relaxation dynamics and the vibrational modes involved.

The electronic structure of **Maleimide** is described in detailed in ref. 49. Briefly, at the ground state optimised geometry the two lowest excited singlet states S_1 and S_2 are at $E(S_1) = 4.07$ eV and $E(S_2) = 4.84$ eV, respectively and are excitations from the oxygen lone pairs to a $\pi^\star$ anti-bonding orbital. S_3 and S_4 are at $E(S_3) = 5.23$ eV and $E(S_2) = 6.70$ eV and correspond to excitations from a π orbital to the same $\pi^\star$ anti-bonding orbital. The electronic structure at the ground state minimum is reported in Table S19 (ESI†), while the orbitals involved are shown in Fig. S4 (ESI†).

To estimate the GAP from the reported excited states, special attention needs to be taken while optimising each excited states. Indeed, κ and $\kappa^\star$ must be computed at the Franck–Condon and minimum geometries of a same diabatic state, *i.e.* the electronic nature of the state must be the same. As reported by Worth *et al.* S_2 and S_3 electronic states cross and therefore generate two minima of different nature in the S_2 PES. In order to avoid any confusion, we will refer to the adiabatic computed states as S_1, S_2, S_3 and S_4 and to the diabatic states by their electronic nature. To alleviate the notations and because the electronic transition associated to each diabatic states is population the same π orbital, we will name the diabatic states by the orbital the electron is excited from, *i.e.* S_{n_2}, S_{n_1}, S_{π_1} or S_{π_2}.

Scans along interpolated coordinates between the ground state and optimised S_k^{Min} geometries are shown in Fig. S5 (ESI†) and emphasize the crossing between S_{n_1} and S_{π_2}. Other crossings between states can be observed, but only at higher

energies, therefore not affecting the minima of the potentials. The electronic structure of **Maleimide** at each of the excited states' minima is shown in Table S20 (ESI†).

The anharmonicity analysis yields small GAPs for each of the lowest singlet states, namely, $\Xi_{S_{n_2}} = 14\%$, $\Xi_{S_{n_1}} = 6\%$, $\Xi_{S_{\pi_2}} = 8\%$ and $\Xi_{S_{\pi_3}} = 6\%$. These values are slightly larger than the values for **TBPe** reflecting an increase in anharmonicity despite the apparent rigidity of **Maleimide**. Fig. S6 (ESI†) shows the potential of the ground and four lowest excited states along the a_1 normal modes, *i.e.* with $\kappa \neq 0$. The curvature of the ground electronic states is systematically overestimated, especially for low-frequency normal modes. While a deviation of the curvature of the electronic excited states from the ground states frequency, can be due to vibronic coupling between excited states, a deviation of the curvature of the ground state from the LVC model is a direct signature of anharmonicity. The RSMA analysis of **Maleimide** is shown in Fig. 2c and d. The normal mode exhibiting the largest ξ is mode ν_{21} that corresponds to a symmetric stretching of C=O. The small ξ for non fully symmetric normal modes reflects the quasi-C_{2v} symmetry of the four lowest excited state minima.

While the GAP remains small, anharmonicity is clearly playing a role in these potentials. Consequently, to assess the effect of the anharmonicity especially on the excited state dynamics, we build two model diabatic Hamiltonians using the LVC approach and compare these to the Hamiltonians previously published by Worth *et al.*[49] and constructed using a fitting procedure of the QVC approximation. The Hamiltonians include the lowest five singlet states, *i.e.* the ground and the four lowest excited states and either 6 or 12 normal modes, full details of the two Hamiltonian are given in Tables S25–S30 (ESI†).

Fig. 3 shows the population kinetics along the dynamics using the Hamiltonians containing 6 (dashed lines) and 12 (full lines) normal modes. In both cases, the simulations are initiated with the wavepacket vertically excited from the ground state geometry vertically into the S_3 state. In the 6-modes model, ultrafast population from S_3 to S_2 is observed within 10 fs. The population then oscillates between the S_3 and S_2 states as there are no normal modes present which couple these states to the lowest S_1 state. S_4 is only marginally populated through the dynamics as it can only receive population from the energetically distant S_2 and S_1 as the S_3 state is of same symmetry as S_4 (A_1) and therefore coupling is symmetry forbidden. In the 12-modes dynamics, the initial population transfer from S_3 to S_2 is still observed, but due to the inclusion of b_2 mode Q_{20}, population within S_2 is quickly transferred into the S_1 state. As before, S_4 receives only a very small amount of population. An equilibrium between the three (S_1, S_2 and S_3) states is reached within 50 fs with the S_2 and S_3 state both exhibiting $\simeq 15\%$ of the total population each, reflecting their near degeneracy.

Both the 6- and 12-modes dynamics offer good agreement with dynamics reported by Worth *et al.*[49] using the QVC approach. For the 6 model model, small differences are observed in the frequency of the oscillations observed between the S_3 and S_2 states which are slightly slower and larger in
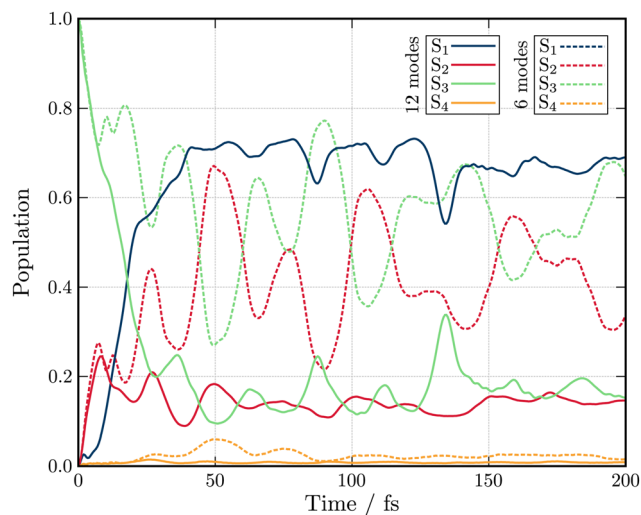
7200 | *Phys. Chem. Chem. Phys.*, 2023, **25**, 7195–7204

This journal is © the Owner Societies 2023

Fig. 3 Excited state population dynamics of **maleimide** after excitation in S_3 ($^1B_2$) state. The two models include 6 (dashed lines) and 12 (full lines) nuclear degrees of freedom.
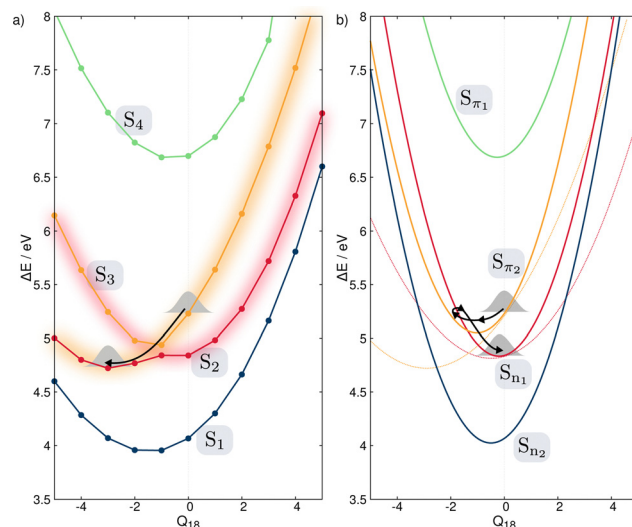

Fig. 4 PES of the ground and four lowest excited singlet states along normal mode Q_{18}. (a) Calculated adiabatic PES. The change of the electronic nature of S_2 and S_3 is emphasized by the change of the diffuse color. (b) Diabatic electronic states built from the LVC approach. The dashed lines qualitatively represent the diabatic states built from following the nature of the electronic states along the adiabatic states shown in (a).
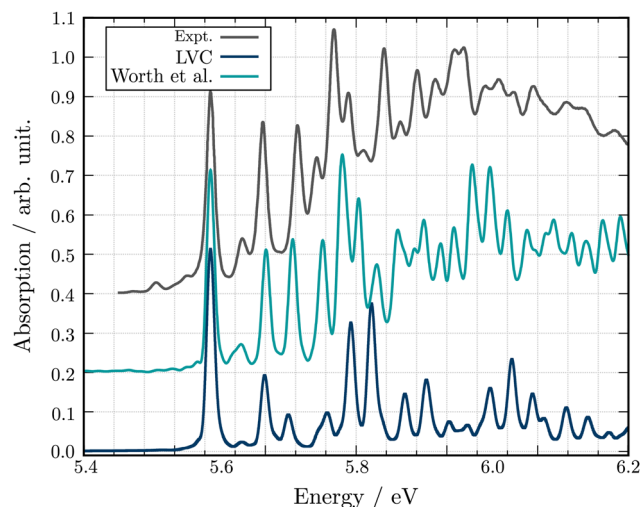
amplitude than those observed within the QVC approach.[49] In the 12 mode model, similar differences are observed, especially in the oscillations in the population of the S_1 state. While this observation could justify the usage of the LVC model for the construction of the model Hamiltonian, the topology of the excited states must be investigated.

Fig. 4 shows the comparison between the computed adiabatic and the diabatic potential energy curves built using the LVC approach of S_1 to S_4 along normal mode Q_{18}. This normal mode is especially important for the dynamics as it creates a conical intersection (CI) between the PES of S_2 and S_3. The topology of the CI (Fig. 4a) obtained from the calculated adiabatic excited state energies is peaked[72,73] and consequently, a wavepacket passing through the CI originating from the FC region would end up in the minimum of diabatic state with a similar nature according to the Landau–Zener principle.[74,75] In contrast the LVC potential (Fig. 4b) along this mode generates a CI topology which is sloped.[72,73] Consequently, a wavepacket would end up in a different minimum exhibiting different character and dynamics. This is highlighted in Fig. 4 where the schematic arrows represent the main direction of the wavepacket upon relaxation. This emphasises that while the population kinetics of the LVC model may appear unchanged compared to a higher order expansion, suggesting that a GAP of $\sim$10% corresponds to a valid LVC, care must be already be taken during the interpretation of these dynamics that the similarity observed in the populations kinetics occurs for the same reason. Indeed, while quantities such as population kinetics are useful, a more rigorous assessment of the accuracy of a potential energy surface is often achieved by calculating observables such as absorption spectra. Fig. 5 shows the second absorption band of **Maleimide** obtained by the Fourier transform of the autocorrelation function of a wavepacket initially placed in S_4. It is compared to the experimental spectrum[49] and the spectrum obtained with the

Fig. 5 Experimental and theoretical absorption spectra for the second excitation band of **Maleimide**. The spectra obtained in this work is shown in blue. The spectrum extracted from the 12 modes dynamics of ref. 49 is shown in turquoise. All spectra have been shifted and scaled to align the first absorption peak in position and intensity to the experimental value.

12 modes Hamiltonian in ref. 49. While the spectrum obtained within the LVC approximation shows qualitative agreement with the spectrum obtained from Worth *et al.* it fails to reproduce the relative intensity between the peaks. The absorption peaks are also sightly shifted and the Gaussian envelope of the absorption band is not well reproduced. This can be attributed to the absence of anharmonicity in the LVC model. In this case, the calculated spectra incorporates peaks >0.5 eV above the absorption band onset, where anharmonicity will

This journal is © the Owner Societies 2023

Phys. Chem. Chem. Phys., 2023, **25**, 7195–7204 | **7201**
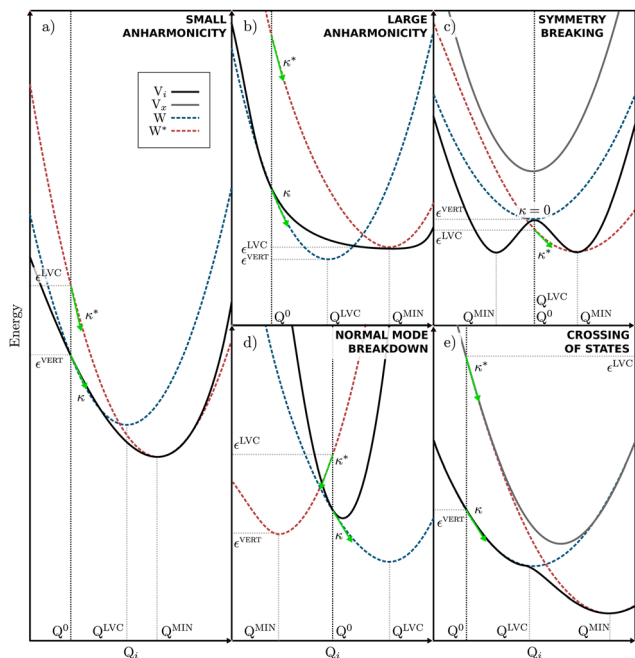
Fig. 6 Possible anharmonicity scenarios. The full black line represents the adiabatic energy of the state of interest (V_i) and a full gray line represents any other state involved in the scenario (V_x). Dashed blue and red lines represent the diabatic states built from either κ (W) or the minimum of V_i (W^*). Green arrows represent the electronic gradients at FC and correspond to κ and κ^*. Q^0, Q^{LVC} and Q^{MIN} correspond to the FC, to the minimum of W and the minimum of V_i, respectively. ε^{vert} is the vertical excitation energy of V_i and ε^{LVC} is the energy at FC of W^*.

play an increasing important role, this is highlighted by the disagreement between the experimental and both calculated spectra with appears to increase with energy.

4 Conclusion

Quantum dynamics simulations are a key theoretical tool for describing processes occurring in electronically excited states, but one of the key challenges for these simulations is obtaining an accurate description of the high-dimensional excited state PES upon which the nuclei evolve. The LVC model is a very compact and efficient model which can be parameterised from relatively few quantum chemistry calculations. However, despite these advantages, the model is based upon coupled-shifted Harmonic oscillators and therefore its validity will be severely tested when larger amplitude motions are present in the excited state dynamics.

For clarity shows some limiting cases of the LVC are shown in Fig. 6. Initially, Fig. 6a illustrates a situation where the LVC approach will remain valid; *i.e* where small anharmonicity of the potential that leads to a small Ξ. In contrast Fig. 6b–e shows four cases that will lead to a large Ξ and the breakdown of the LVC approach, namely (b) a large anharmonicity of the potential, (c) a symmetry breaking in the excited states, (d) a breakdown of the normal mode representation, *i.e.* the normal modes change nature between the FC and the excited state minimum geometries, and (e) the crossing of electronic states.

In this paper we have introduced and tested a metric, the Global Anharmonicity Parameter (GAP), which can be used to assess the accuracy of an LVC potential. This is based upon assessing the differences between the intrastate coupling constant, κ which can be calculated in two ways. If both yield the same results, the harmonic approximation upon which the LVC is based is valid. We have assessed the performance of this metric using three molecules, namely **TBPe**, **TAT-3DBTO$_2$** and **Maleimide**. The first two illustrate two clear examples when the LVC is valid and breakdowns, respectively. The potential for **Maleimide** illustrates an interesting case. Indeed, it displays a relatively small GAP, $\sim$10% and the excited state dynamics calculated using the LVC potential is in good agreement with those previously obtained using the QVC approach:[49] However, the approximations made in the LVC change the nature of the interaction between the coupled states meaning that although the population dynamics remains very similar to higher level approaches, the mechanism leading to the dynamics is different.

In conclusion, we have demonstrated that the GAP is a useful metric for assessing the validity of the LVC approximation. From the present work, it appears that a GAP of $\geq$10% means any simulations using the LVC should be treated with caution. The validity of the LVC and impact of the corresponding GAP value can be assessed by calculating experimental observables, such as absorption spectra. Although further work on a broader range of systems would be required to provide insights into the effect of the magnitude of this metric, this provides an important basis for future works using the LVC approximation.

Conflicts of interest

There are no conflicts to declare.

Acknowledgements

References

1 J. Gibson, A. P. Monkman and T. J. Penfold, *ChemPhysChem*, 2016, **17**, 2956–2961.
2 T. Northey and T. Penfold, *Org. Electron.*, 2018, **59**, 45–48.
3 H. Tamura and I. Burghardt, *J. Am. Chem. Soc.*, 2013, **135**, 16364–16367.
4 H. Tamura and I. Burghardt, *J. Phys. Chem. C*, 2013, **117**, 15020–15025.
5 H. Tamura, I. Burghardt and M. Tsukada, *J. Phys. Chem. C*, 2011, **115**, 10205–10210.

7202 | *Phys. Chem. Chem. Phys.*, 2023, **25**, 7195–7204

This journal is © the Owner Societies 2023

6   M. H. Beck, A. Jäckle, G. A. Worth and H.-D. Meyer, *Phys. Rep.*, 2000, **324**, 1–105.

7   H.-D. Meyer, F. Gatti and G. A. Worth, *Multidimensional quantum dynamics: MCTDH theory and applications*, John Wiley & Sons, 2009.

8   J. C. Tully and R. K. Preston, *J. Chem. Phys.*, 1971, **55**, 562–572.

9   J. C. Tully, *J. Chem. Phys.*, 1990, **93**, 1061–1071.

10 T. J. Martinez, M. Ben-Nun and R. Levine, *J. Phys. Chem. A*, 1996, **100**, 7884–7895.

11 M. Ben-Nun and T. J. Martnez, *J. Chem. Phys.*, 1998, **108**, 7244–7257.

12 D. V. Shalashilin and M. S. Child, *Chem. Phys.*, 2004, **304**, 103–120.

13 D. V. Shalashilin, *J. Chem. Phys.*, 2009, **130**, 244101.

14 D. V. Makhov, W. J. Glover, T. J. Martinez and D. V. Shalashilin, *J. Chem. Phys.*, 2014, **141**, 054110.

15 G. Richings, I. Polyak, K. Spinlove, G. Worth, I. Burghardt and B. Lasorne, *Int. Rev. Phys. Chem.*, 2015, **34**, 269–308.

16 G. Christopoulou, A. Freibert and G. A. Worth, *J. Chem. Phys.*, 2021, **154**, 124127.

17 E. J. Heller, *J. Chem. Phys.*, 1975, **62**, 1544–1555.

18 E. J. Heller, *J. Chem. Phys.*, 1981, **75**, 2923–2931.

19 S.-Y. Lee and E. J. Heller, *J. Chem. Phys.*, 1982, **76**, 3035–3044.

20 B. F. Curchod and T. J. Martnez, *Chem. Rev.*, 2018, **118**, 3305–3336.

21 R. Crespo-Otero and M. Barbatti, *Chem. Rev.*, 2018, **118**, 7026–7068.

22 O. Vendrell, F. Gatti, D. Lauvergnat and H.-D. Meyer, *J. Chem. Phys.*, 2007, **127**, 184302.

23 B. J. Braams and J. M. Bowman, *Int. Rev. Phys. Chem.*, 2009, **28**, 577–606.

24 J. M. Bowman, G. Czako and B. Fu, *Phys. Chem. Chem. Phys.*, 2011, **13**, 8094–8111.

25 B. F. Curchod, U. Rothlisberger and I. Tavernelli, *ChemPhysChem*, 2013, **14**, 1314–1340.

26 H. Köppel, W. Domcke and L. S. Cederbaum, *Conical Intersections*, 2004, 323–367.

27 L. S. Cederbaum, H. Köppel and W. Domcke, *Int. J. Quantum Chem.*, 2009, **20**, 251–267.

28 T. J. Penfold, E. Gindensperger, C. Daniel and C. M. Marian, *Chem. Rev.*, 2018, **118**, 6975–7025.

29 S. Thompson, J. Eng and T. Penfold, *J. Chem. Phys.*, 2018, **149**, 014304.

30 Y. Harabuchi, J. Eng, E. Gindensperger, T. Taketsugu, S. Maeda and C. Daniel, *J. Chem. Theory Comput.*, 2016, **12**, 2335–2345.

31 J. P. Zobel, M. Heindl, F. Plasser, S. Mai and L. González, *Acc. Chem. Res.*, 2021, **54**, 3760–3771.

32 S. Mai, P. Marquetand and L. González, *J. Chem. Phys.*, 2014, **140**, 204302.

33 S. Gómez, M. Heindl, A. Szabadi and L. González, *J. Phys. Chem. A*, 2019, **123**, 8321–8332.

34 G. Capano, M. Chergui, U. Rothlisberger, I. Tavernelli and T. J. Penfold, *J. Phys. Chem. A*, 2014, **118**, 9861–9869.

35 M. Pápai, G. Vankó, T. Rozgonyi and T. J. Penfold, *J. Phys. Chem. Lett.*, 2016, **7**, 2009–2014.

36 J. P. Zobel, T. Knoll and L. González, *Chem. Sci.*, 2021, **12**, 10791–10801.

37 G. Capano, T. Penfold, M. Chergui and I. Tavernelli, *Phys. Chem. Chem. Phys.*, 2017, **19**, 19590–19600.

38 M. Pápai, T. J. Penfold and K. B. Møller, *J. Phys. Chem. C*, 2016, **120**, 17234–17241.

39 Q. Xu, D. Aranda, M. Yaghoubi Jouybari, Y. Liu, M. Wang, J. Cerezo, R. Improta and F. Santoro, *J. Phys. Chem. A*, 2022, **126**, 7468–7479.

40 M. Y. Jouybari, J. A. Green, R. Improta and F. Santoro, *J. Phys. Chem. A*, 2021, **125**, 8912–8924.

41 J. A. Green, M. Yaghoubi Jouybari, H. Asha, F. Santoro and R. Improta, *J. Chem. Theory Comput.*, 2021, **17**, 4660–4674.

42 F. Aleotti, D. Aranda, M. Yaghoubi Jouybari, M. Garavelli, A. Nenov and F. Santoro, *J. Chem. Phys.*, 2021, **154**, 104106.

43 D. Aranda and F. Santoro, *J. Chem. Theory Comput.*, 2021, **17**, 1691–1700.

44 Y. Giret, J. Eng, T. Pope and T. Penfold, *J. Mater. Chem. C*, 2021, **9**, 1362–1369.

45 J. Eng and T. J. Penfold, *Chem. Record*, 2020, **20**, 831–856.

46 J. Eng and T. J. Penfold, *Commun. Chem.*, 2021, **4**, 1–4.

47 P. L. Dos Santos, J. S. Ward, D. G. Congrave, A. S. Batsanov, J. Eng, J. E. Stacey, T. J. Penfold, A. P. Monkman and M. R. Bryce, *Adv. Sci.*, 2018, **5**, 1700989.

48 J. Eng, J. Hagon and T. J. Penfold, *J. Mater. Chem. C*, 2019, **7**, 12942–12952.

49 A. Lehr, S. Gómez, M. A. Parkes and G. A. Worth, *Phys. Chem. Chem. Phys.*, 2020, **22**, 25272–25283.

50 Y. Giret, J. Eng, T. Pope and T. Penfold, *J. Mater. Chem. C*, 2021, **9**, 1362–1369.

51 VCMAKER, 2022, **github.com/JulienEng/VCMaker**.

52 Y. Shao, Z. Gan, E. Epifanovsky, A. T. Gilbert, M. Wormit, J. Kussmann, A. W. Lange, A. Behn, J. Deng, X. Feng, D. Ghosh, M. Goldey, P. R. Horn, L. D. Jacobson, I. Kaliman, R. Z. Khaliullin, T. Kuś, A. Landau, J. Liu, E. I. Proynov, Y. M. Rhee, R. M. Richard, M. A. Rohrdanz, R. P. Steele, E. J. Sundstrom, H. L. Woodcock, P. M. Zimmerman, D. Zuev, B. Albrecht, E. Alguire, B. Austin, G. J. O. Beran, Y. A. Bernard, E. Berquist, K. Brandhorst, K. B. Bravaya, S. T. Brown, D. Casanova, C.-M. Chang, Y. Chen, S. H. Chien, K. D. Closser, D. L. Crittenden, M. Diedenhofen, R. A. DiStasio, H. Do, A. D. Dutoi, R. G. Edgar, S. Fatehi, L. Fusti-Molnar, A. Ghysels, A. Golubeva-Zadorozhnaya, J. Gomes, M. W. Hanson-Heine, P. H. Harbach, A. W. Hauser, E. G. Hohenstein, Z. C. Holden, T.-C. Jagau, H. Ji, B. Kaduk, K. Khistyaev, J. Kim, J. Kim, R. A. King, P. Klunzinger, D. Kosenkov, T. Kowalczyk, C. M. Krauter, K. U. Lao, A. D. Laurent, K. V. Lawler, S. V. Levchenko, C. Y. Lin, F. Liu, E. Livshits, R. C. Lochan, A. Luenser, P. Manohar, S. F. Manzer, S.-P. Mao, N. Mardirossian, A. V. Marenich, S. A. Maurer, N. J. Mayhall, E. Neuscamman, C. M. Oana, R. Olivares-Amaya, D. P. ONeill, J. A. Parkhill, T. M. Perrine, R. Peverati, A. Prociuk, D. R. Rehn, E. Rosta, N. J. Russ, S. M. Sharada, S. Sharma, D. W. Small,

This journal is © the Owner Societies 2023

Phys. Chem. Chem. Phys., 2023, **25**, 7195–7204 | 7203

A. Sodt, T. Stein, D. Stück, Y.-C. Su, A. J. Thom, T. Tsuchimochi, V. Vanovschi, L. Vogt, O. Vydrov, T. Wang, M. A. Watson, J. Wenzel, A. White, C. F. Williams, J. Yang, S. Yeganeh, S. R. Yost, Z.-Q. You, I. Y. Zhang, X. Zhang, Y. Zhao, B. R. Brooks, G. K. Chan, D. M. Chipman, C. J. Cramer, W. A. Goddard, M. S. Gordon, W. J. Hehre, A. Klamt, H. F. Schaefer, M. W. Schmidt, C. D. Sherrill, D. G. Truhlar, A. Warshel, X. Xu, A. Aspuru-Guzik, R. Baer, A. T. Bell, N. A. Besley, J.-D. Chai, A. Dreuw, B. D. Dunietz, T. R. Furlani, S. R. Gwaltney, C.-P. Hsu, Y. Jung, J. Kong, D. S. Lambrecht, W. Liang, C. Ochsenfeld, V. A. Rassolov, L. V. Slipchenko, J. E. Subotnik, T. Van Voorhis, J. M. Herbert, A. I. Krylov, P. M. Gill and M. Head-Gordon, *Mol. Phys.*, 2014, **113**, 184–215.

53 E. Epifanovsky, A. T. B. Gilbert, X. Feng, J. Lee, Y. Mao, N. Mardirossian, P. Pokhilko, A. F. White, M. P. Coons, A. L. Dempwolff, Z. Gan, D. Hait, P. R. Horn, L. D. Jacobson, I. Kaliman, J. Kussmann, A. W. Lange, K. U. Lao, D. S. Levine, J. Liu, S. C. McKenzie, A. F. Morrison, K. D. Nanda, F. Plasser, D. R. Rehn, M. L. Vidal, Z.-Q. You, Y. Zhu, B. Alam, B. J. Albrecht, A. Aldossary, E. Alguire, J. H. Andersen, V. Athavale, D. Barton, K. Begam, A. Behn, N. Bellonzi, Y. A. Bernard, E. J. Berquist, H. G. A. Burton, A. Carreras, K. Carter-Fenk, R. Chakraborty, A. D. Chien, K. D. Closser, V. Cofer-Shabica, S. Dasgupta, M. de Wergifosse, J. Deng, M. Diedenhofen, H. Do, S. Ehlert, P.-T. Fang, S. Fatehi, Q. Feng, T. Friedhoff, J. Gayvert, Q. Ge, G. Gidofalvi, M. Goldey, J. Gomes, C. E. González-Espinoza, S. Gulania, A. O. Gunina, M. W. D. Hanson-Heine, P. H. P. Harbach, A. Hauser, M. F. Herbst, M. Hernández Vera, M. Hodecker, Z. C. Holden, S. Houck, X. Huang, K. Hui, B. C. Huynh, M. Ivanov, Á. Jász, H. Ji, H. Jiang, B. Kaduk, S. Kähler, K. Khistyaev, J. Kim, G. Kis, P. Klunzinger, Z. Koczor-Benda, J. H. Koh, D. Kosenkov, L. Koulias, T. Kowalczyk, C. M. Krauter, K. Kue, A. Kunitsa, T. Kus, I. Ladjánszki, A. Landau, K. V. Lawler, D. Lefrancois, S. Lehtola, R. R. Li, Y.-P. Li, J. Liang, M. Liebenthal, H.-H. Lin, Y.-S. Lin, F. Liu, K.-Y. Liu, M. Loipersberger, A. Luenser, A. Manjanath, P. Manohar, E. Mansoor, S. F. Manzer, S.-P. Mao, A. V. Marenich, T. Markovich, S. Mason, S. A. Maurer, P. F. McLaughlin, M. F. S. J. Menger, J.-M. Mewes, S. A. Mewes, P. Morgante, J. W. Mullinax, K. J. Oosterbaan, G. Paran, A. C. Paul, S. K. Paul, F. Pavošević, Z. Pei, S. Prager, E. I. Proynov, Á. Rák, E. Ramos-Cordoba, B. Rana, A. E. Rask, A. Rettig, R. M. Richard, F. Rob, E. Rossomme, T. Scheele, M. Scheurer, M. Schneider, N. Sergueev, S. M. Sharada, W. Skomorowski, D. W. Small, C. J. Stein, Y.-C. Su, E. J. Sundstrom, Z. Tao, J. Thirman, G. J. Tornai, T. Tsuchimochi, N. M. Tubman, S. P. Veccham, O. Vydrov, J. Wenzel, J. Witte, A. Yamada, K. Yao, S. Yeganeh, S. R. Yost, A. Zech, I. Y. Zhang, X. Zhang, Y. Zhang, D. Zuev, A. Aspuru-Guzik, A. T. Bell, N. A. Besley, K. B. Bravaya, B. R. Brooks, D. Casanova, J.-D. Chai, S. Coriani, C. J. Cramer, G. Cserey, A. E. DePrince, R. A. DiStasio, A. Dreuw, B. D. Dunietz, T. R. Furlani, W. A. Goddard, S. Hammes-Schiffer, T. Head-Gordon, W. J. Hehre, C.-P. Hsu, T.-C. Jagau, Y. Jung, A. Klamt, J. Kong, D. S. Lambrecht, W. Liang, N. J. Mayhall, C. W. McCurdy, J. B. Neaton, C. Ochsenfeld, J. A. Parkhill, R. Peverati, V. A. Rassolov, Y. Shao, L. V. Slipchenko, T. Stauch, R. P. Steele, J. E. Subotnik, A. J. W. Thom, A. Tkatchenko, D. G. Truhlar, T. Van Voorhis, T. A. Wesolowski, K. B. Whaley, H. L. Woodcock, P. M. Zimmerman, S. Faraji, P. M. W. Gill, M. Head-Gordon, J. M. Herbert and A. I. Krylov, *J. Chem. Phys.*, 2021, **155**, 084801.

54 C. Adamo and V. Barone, *J. Chem. Phys.*, 1999, **110**, 6158–6170.

55 F. Weigend and R. Ahlrichs, *Phys. Chem. Chem. Phys.*, 2005, **7**, 3297.

56 S. Hirata and M. Head-Gordon, *Chem. Phys. Lett.*, 1999, **314**, 291–299.

57 M. A. Rohrdanz, K. M. Martins and J. M. Herbert, *J. Chem. Phys.*, 2009, **130**, 054112.

58 R. Ditchfield, W. J. Hehre and J. A. Pople, *J. Chem. Phys.*, 1971, **54**, 724–728.

59 W. J. Hehre, R. Ditchfield and J. A. Pople, *J. Chem. Phys.*, 1972, **56**, 2257–2261.

60 P. Hariharan and J. Pople, *Mol. Phys.*, 1974, **27**, 209–214.

61 T. J. Penfold, *J. Phys. Chem. C*, 2015, **119**, 13535–13544.

62 E. Livshits and R. Baer, *Phys. Chem. Chem. Phys.*, 2007, **9**, 2932.

63 H. Sun, C. Zhong and J.-L. Brédas, *J. Chem. Theory Comput.*, 2015, **11**, 3851–3858.

64 J. Eng, B. A. Laidlaw and T. J. Penfold, *J. Comput. Chem.*, 2019, **40**, 2191–2199.

65 D. E. Woon and T. H. Dunning, *J. Chem. Phys.*, 1993, **98**, 1358–1371.

66 S. A. Ahmad, J. Eng and T. J. Penfold, *J. Mater. Chem. C*, 2022, **10**, 4785–4794.

67 T. J. Penfold and J. Eng, *ChemPhotoChem*, 2021, e202200243.

68 J. von Sonntag and W. Knolle, *J. Photochem. Photobiol., A*, 2000, **136**, 133–139.

69 C. Antczak, B. Bauvois, C. Monneret and J.-C. Florent, *Bioorg. Med. Chem.*, 2001, **9**, 2843–2848.

70 D. M. Davies, C. Murray, M. Berry, A. J. Orr-Ewing and K. I. Booker-Milburn, *J. Org. Chem.*, 2007, **72**, 1449–1457.

71 L. M. Tedaldi, A. E. Aliev and J. R. Baker, *Chem. Commun.*, 2012, **48**, 4725–4727.

72 D. R. Yarkony, *Rev. Mod. Phys.*, 1996, **68**, 985–1013.

73 S. Matsika, *Chem. Rev.*, 2021, **121**, 9407–9449.

74 L. Landau and E. Lifshitz, in *Perspectives in Theoretical Physics*, ed. L. Pitaevski, Pergamon, Amsterdam, 1992, pp. 287–297.

75 C. Zener and R. H. Fowler, *Proc. R. Soc. London, Ser. A*, 1932, **137**, 696–702.

7204 | *Phys. Chem. Chem. Phys.*, 2023, **25**, 7195–7204

This journal is © the Owner Societies 2023